Available online at www.sciencedirect.com
ScienceDirect
Journal of Sound and Vibration 316 (2008) 122–136
JOURNAL OF SOUND AND VIBRATION
www.elsevier.com/locate/jsvi

Reconstruction of distributed dynamic loads on an Euler beam via mode-selection and consistent spatial expression

X.Q. Jiang, H.Y. Hu*

MOE Key Laboratory of Structure Mechanics and Control for Aircraft, Nanjing University of Aeronautics and Astronautics, 210016 Nanjing, China

Received 6 October 2007; received in revised form 18 February 2008; accepted 20 February 2008
Handling Editor: J. Lam
Available online 3 April 2008

Abstract

The paper presents a new approach to reconstruct the distributed dynamic loads on an Euler beam from the beam response. The approach is based on a mode-selection method and an idea of consistent spatial expression for the distributed dynamic loads, and is supported by error estimation. The idea of the optimal range of frequency and spatial modes for load reconstruction is proposed and verified by numerical simulations. To cope with the tough problem of identifying the dynamic loads near a fixed boundary, the concept of consistent spatial expression for the dynamic loads is put forward, and the Legendre polynomials are used as the consistent orthogonal base functions to describe the distributed dynamic loads. The numerical simulations show that the reconstruction accuracy near the fixed boundaries can be greatly enhanced.

1. Introduction

The identification of dynamic loads on a structure is of great practical interest in aerospace engineering, mechanical engineering, civil engineering and so on because a prior knowledge of the dynamic loads is essential for the design, analysis and evaluation of the structure, while the direct measurements of dynamic loads are often not feasible in practice. The past decade has witnessed numerous studies of identifying the dynamic loads on a system of multiple degrees of freedom [1–4], the moving loads on a bridge [5,6], and impulsive load or multi-point load on a continuum [7–9]. The identification of spatially distributed dynamic loads on a continuum is relatively new [10–14]. For instance, Liu and Shepard [11] studied the reconstruction of harmonic force applied on a beam, while Granger and Perotin [14] investigated the identification of the random excitation on a beam. In these two studies, they introduced and used similar but different ideas of modified modal expression for beam dynamics. Pezerat and Guyader [13] studied the reconstruction of harmonic excitation acting on a rectangular plate, and Djamaa et al. [10] studied the load on a thin cylindrical shell. In both studies, they used the model of finite elements to describe the plate and the shell. Furthermore,

*Corresponding author. Tel.: +86 25 8489 1672; fax: +86 25 8489 1512.
E-mail address: hyhu@nuaa.edu.cn (H.Y. Hu).

0022-460X/$ - see front matter © 2008 Elsevier Ltd. All rights reserved.
doi:10.1016/j.jsv.2008.02.038

Sehlstedt [12] investigated a seemingly different problem to reconstruct the boundary traction on a constrained structure.

The reconstruction of distributed dynamic loads on a continuum is a complex inverse problem with inherent ill-posedness. However, it is not clear whether the ill-posedness results from physics or mathematics. In engineering practice, to reconstruct the distributed dynamic loads on a continuum is an expansive mapping process of deducing continuous integrated load information from discrete parts of response information, which makes the problem so involved that many aspects have to be dealt with. In the studies mentioned above and some others, much attention was paid to the complicated technical problems in mathematics, especially in the ill-posedness and regularization methods [15–22], while less consideration was put to the physical nature of the problem.

This paper is mainly concerned with some physical aspects of the identification of distributed dynamic loads. For example, attention will be paid to whether or not the distributed dynamic loads on a continuum can be reconstructed integrally from the response data by inverse inference. A reasonable extension of this question is that the reconstruction of distributed dynamic loads can be made only in part. From the viewpoint of the forward problem from the dynamic load to the dynamic response, the continuum acts as a transducer with the inherent physical property of smoothness. That is, the continuum behaves like an inverse transducer that enlarges the unevenness in response information. Thus, the continuum as an inverse transducer is naturally ill-posed in physics, instead of in mathematics only. In addition, attention will be paid to the following questions. Will the above fact suggest that the reconstruction of distributed dynamic loads on a continuum can be solved only in part? To what degree can the result of the reconstruction be controlled? Will it be different when a strategy intending in advance to obtain only some limited range of the load information is adopted?

In practice, the measurements of dynamic response are often not enough for the reconstruction of dynamic loads. Consequently, many studies have focused on the additional information. However, it does not seem an efficient policy. In this study, an idea of drawing the inner relation between the temporal and spatial information from the measurements will be considered so as to establish a strong linkage between the temporal response data and the spatial response data, since they are through the same system and are parts of the integrated response information.

For simplicity, this study will focus on the reconstruction of the dynamic loads on an undamped Euler beam so as to clarify some phenomena in the inverse problem of reconstructing distributed dynamic loads on a continuum from discrete response data. The rest of the paper is organized as follows. In Section 2, a concept of ''scale effect'' is first proposed to reveal the relation between the temporal and spatial information in the beam response, and then it is applied to the ''mode selection'' approach to determine the appropriate range for the load reconstruction with acceptable accuracy. In the previous studies of reconstructing the dynamic loads on a beam [11,14], the modified modal functions were employed to describe the distributed dynamic loads. With regard to simply supported boundary conditions, the modal functions, including the modified modal functions, gradually tend to be zero near the fixed boundary and conflict with the dynamic loads not vanishing near the fixed boundary. In Section 3, therefore, a concept of ''consistent spatial expression for distributed dynamic loads'' is suggested to cope with the boundary problem. In Section 4, several numerical simulations will be given to demonstrate the theoretical results in Sections 2 and 3. Finally, some concluding remarks are made in Section 5.

2. Mode selection

The dynamic response of a uniform undamped Euler beam yields a dimensionless partial differential equation as follows:

$$\frac{(\kappa_1 L)^4}{4\pi^2}\frac{\partial^2 \bar{w}(\bar{x},\bar{t})}{\partial \bar{t}^2}+\frac{\partial^4 \bar{w}(\bar{x},\bar{t})}{\partial \bar{x}^4}=\bar{f}(\bar{x},\bar{t}), \tag{1}$$

where $\bar{x}\equiv x/L$ is the dimensionless spatial variable scaled by the length L of beam, $\bar{t}\equiv t/T_1$ the dimensionless time scaled by $T_1\equiv 2\pi/\omega_1$, $\omega_1\equiv \kappa_1^2\sqrt{EI/\rho A}$, $\bar{w}\equiv w/L$ the dimensionless translational displacement, $\bar{f}\equiv L^3 f/(EI)$ the dimensionless external transverse excitation, κ_1 the circular wavenumber of the first modal

shape, ρ the density of beam material, E the Young's modulus of beam material, A the area of cross section of beam, and I the second moment of the area, respectively.

With the use of modal transformation $\bar{w}(\bar{x},\bar{t})=\sum_{m=1}^{\infty}W_m(\bar{x})q_m(\bar{t})$, the mth modal response corresponding to Eq. (1) becomes

$$\ddot{q}_m(\bar{t})+\bar{\omega}_m^2 q_m(\bar{t})=\frac{4\pi^2}{(\kappa_1 L)^4}\bar{f}_m(t), \tag{2}$$

where the dot represents the derivative with respect to the dimensionless time $\bar{t}$, $q_m(\bar{t})$ is the modal coordinate, $\bar{f}_m(\bar{t})\equiv\int_0^1 W_m(\bar{x})\bar{f}(\bar{x},\bar{t})\,\mathrm{d}\bar{x}$ the general force, and $W_m(\bar{x})$ the mode shape, respectively.

If the transverse excitation is harmonic in the time domain and proportional to the jth mode shape in the spatial domain, namely

$$\bar{f}(\bar{x},\bar{t})=cW_j(\bar{x})\mathrm{e}^{\mathrm{i}\bar{\omega}\bar{t}}, \tag{3}$$

where c is a positive real constant, the general force and the corresponding steady-state response of the mth mode read

$$\bar{f}_m(\bar{t})=c\delta_{jm}\mathrm{e}^{\mathrm{i}\bar{\omega}\bar{t}}, \tag{4}$$

$$q_m(\bar{t})=c\frac{4\pi^2}{(\kappa_1 L)^4}\delta_{jm}\frac{1}{\bar{\omega}_m^2-\bar{\omega}^2}\mathrm{e}^{\mathrm{i}\bar{\omega}\bar{t}},\quad \ddot{q}_m(\bar{t})=c\frac{4\pi^2}{(\kappa_1 L)^4}\delta_{jm}\frac{1}{1-(\bar{\omega}_m/\bar{\omega})^2}\mathrm{e}^{\mathrm{i}\bar{\omega}\bar{t}}, \tag{5}$$

where δ_{jm} is the Kronecker delta.

To check the scale effect of the variance of both mode order m and excitation frequency $\bar{\omega}$, it is useful to introduce two factors as follows:

$$\mathrm{SF}_{\bar{w}}\equiv\frac{1}{\bar{\omega}_m^2-\bar{\omega}^2},\quad \mathrm{SF}_{\bar{a}}\equiv\frac{1}{1-(\bar{\omega}_m/\bar{\omega})^2}. \tag{6}$$

With the help of $\mathrm{SF}_{\bar{w}}$ and $\mathrm{SF}_{\bar{a}}$, the translational displacement and acceleration of the steady-state response can be expressed as

$$\bar{w}(\bar{x},\bar{t})=c\frac{4\pi^2}{(\kappa_1 L)^4}\mathrm{SF}_{\bar{w}}W_j(\bar{x})\mathrm{e}^{\mathrm{i}\bar{\omega}\bar{t}},\quad \bar{a}(\bar{x},\bar{t})=c\frac{4\pi^2}{(\kappa_1 L)^4}\mathrm{SF}_{\bar{a}}W_j(\bar{x})\mathrm{e}^{\mathrm{i}\bar{\omega}\bar{t}}. \tag{7}$$

For a simply supported Euler beam, $(\kappa_1 L)^4/(4\pi^2)=\pi^2/4$, and the dimensionless circular wavenumber, circular frequency and modal shape of the mth mode are $\bar{\kappa}_m=m\pi$, $\bar{\omega}_m=2m^2\pi$, and $W_m(\bar{x})=\sqrt{2}\sin(\bar{\kappa}_m\bar{x})$, respectively. For the excitation frequency $\bar{\omega}$ between two natural frequencies $\bar{\omega}_k$ and $\bar{\omega}_{k+1}$, where $\bar{\omega}_0$ is defined as $\bar{\omega}_0\equiv 0$, let $\bar{\omega}=\bar{\omega}_k+\Delta\bar{\omega}_k$ and $\Delta\bar{\omega}_k>0$. Then, it is easy to recast Eq. (6) as

$$\mathrm{SF}_{\bar{w}}=\frac{1}{4\pi^2}\frac{1}{(k^2+\beta)^2}\frac{1}{\gamma^2-1},\quad \mathrm{SF}_{\bar{a}}=\frac{1}{1-\gamma^2}, \tag{8}$$

where

$$\beta\equiv\frac{\Delta\bar{\omega}_k}{\bar{\omega}_1},\quad \gamma\equiv\frac{\bar{\omega}_m}{\bar{\omega}}=\frac{m^2}{k^2+\beta},\quad 0<\beta<2k+1. \tag{9}$$

Eq. (8) indicates that the scale effect mainly comes from $c_s\equiv 1/|1-\gamma^2|$, $\gamma\in(0,\infty)$, which is shown in Fig. 1.

Now it is clear that an undamped Euler beam is a low-pass filter in the frequency domain and the modal domain, as may be observed in Eqs. (8) and (9) from the fact that $\mathrm{SF}_{\bar{w}}\to 0$ when $k\to\infty$ but m is fixed, and that $\mathrm{SF}_{\bar{w}}\to 0$ and $\mathrm{SF}_{\bar{a}}\to 0$ when $m\to\infty$ but k and β are fixed. Furthermore, the steady-state response greatly depends on the difference between the excitation frequency and the natural frequencies corresponding to the modal components included in the spatial expression of the excitation. For example, given the harmonic excitation distributed proportionally to a mode shape in the spatial domain, the beam response becomes remarkable if the excitation frequency is close to the natural frequency corresponding to the mode shape. Otherwise, the beam response is imperceptible.

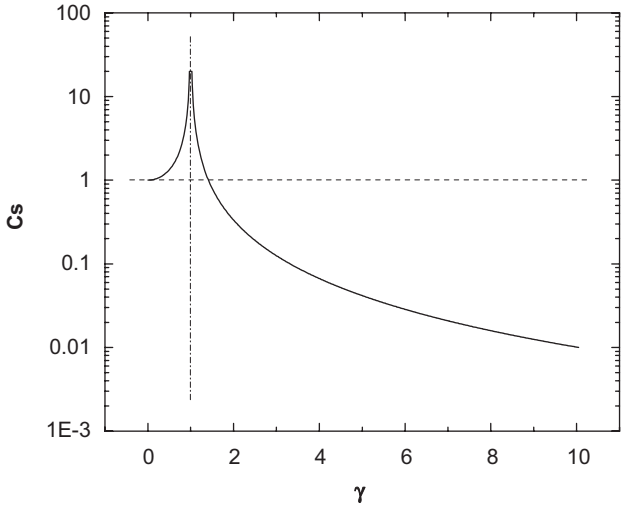

Fig. 1. Cs vs γ.

The reconstruction of distributed dynamic loads on an Euler beam is inherently a process of partial identification when any truncated modal expression is used to describe the beam response. This assertion also holds true for the reconstruction of distributed dynamic loads on any continuum. Hence, the difficulty in reconstructing the dynamic load of high frequency has been well acknowledged. Furthermore, the reconstruction of distributed dynamic loads can only be made in part since the spatial modal components of high wavenumbers have to be truncated according to the above discussion. The above facts lead to a *hypothesis* for the reconstruction of distributed dynamic loads as follows. Only the distributed dynamic loads of a certain range of frequency and spatial modes could be reconstructed from the response data, and there is an optimal range for the reconstruction when a particular level of sensitivity and noise in response measurement is given for a specific beam. Furthermore, the coincidence is that this is analogous to the function of animal's ears, which means different animals have different ranges of sound perception in nature.

Based on this hypothesis, a method named "mode selection" is proposed based on the concept of "scale factor" in Eq. (6) to determine an appropriate range for load reconstruction. When the main frequencies of loads are obtained from the response, the scale factor $SF_{\bar{w}}$ or $SF_{\bar{a}}$ of every mode can be determined, and only those modes, whose corresponding scale factors divided by the maximum scale factor are larger than a threshold, will be chosen for load reconstruction. Section 4 will demonstrate how to determine such a threshold through empirical data in simulations.

This approach seems similar to the regularization method of discarding smaller singular values, but they are not the same concept in fact. When the regularization method is tried to be applied to the process of mode selection, the results are not so good. Furthermore, though the scale effect seems apparent in the forward problem and causes no trouble, it is not the case in the inverse process. This scale effect results in ill-posedness and irreversibility in the inverse problem.

Section 4 gives some numerical simulations to verify the hypothesis. It is hard to depict the cases of the failure to reconstruct the spatial modal components of high wavenumber. However, the numerical results in Section 4 through case studies 1 and 2 show that the reconstruction accuracy is enhanced when an appropriate range is selected. The results there indicate that it is very important to determine an appropriate range of frequency and spatial modes in the load reconstruction, and that the accuracy of reconstructed load greatly decreases if the range is too broad.

3. Reconstruction of distributed dynamic loads and error analysis

Based on the hypothesis stated in Section 2, an improved theory with the help of "mode selection" will be developed in Section 3.1 to reconstruct the distributed dynamic loads on an Euler beam. Furthermore, the

theory, combined with the "consistent spatial expression" for distributed dynamic loads, is used to cope with the tough problem of identifying the distributed dynamic loads near any fixed boundary in Section 3.2. Later, the error evolution of the theory is discussed at length in Section 3.3.

3.1. Theory of the reconstruction of distributed dynamic loads

This subsection deals with the reconstruction of the distributed dynamic loads on a uniform undamped Euler beam governed by Eq. (1). If the dynamic load comprises N_p frequency components in the time domain, it can be expressed as

$$\bar{f}(\bar{x},\bar{t}) = \sum_{r=1}^{N_p} F_r(\bar{x}) e^{i\bar{\omega}_r^* \bar{t}}. \tag{10}$$

The general force and the corresponding steady-state response of the mth mode read

$$\bar{f}_m(\bar{t}) = \sum_{r=1}^{N_p} \int_0^1 W_m(\bar{x}) F_r(\bar{x})\, d\bar{x} e^{i\bar{\omega}_r^* \bar{t}} \tag{11}$$

$$q_m(\bar{t}) = \frac{4\pi^2}{(\kappa_1 L)^4} \sum_{r=1}^{N_p} \frac{1}{\bar{\omega}_m^2 - \bar{\omega}_r^{*2}} \int_0^1 W_m(\bar{x}) F_r(\bar{x}) d\bar{x} e^{i\bar{\omega}_r^* \bar{t}}, \tag{12a}$$

$$\ddot{q}_m(\bar{t}) = \frac{4\pi^2}{(\kappa_1 L)^4} \sum_{r=1}^{N_p} \frac{1}{1 - (\bar{\omega}_m/\bar{\omega}_r^*)^2} \int_0^1 W_m(\bar{x}) F_r(\bar{x})\, d\bar{x} e^{i\bar{\omega}_r^* \bar{t}} \tag{12b}$$

There follows the translational displacement and acceleration of the steady-state response:

$$\bar{w}(\bar{x},\bar{t}) = \sum_{m=1}^{\infty} W_m(\bar{x}) q_m(\bar{t}) = \frac{4\pi^2}{(\kappa_1 L)^4} \sum_{m=1}^{\infty} \sum_{r=1}^{N_p} \frac{1}{\bar{\omega}_m^2 - \bar{\omega}_r^{*2}} \int_0^1 W_m(\bar{x}) F_r(\bar{x}) d\bar{x} W_m(\bar{x}) e^{i\bar{\omega}_r^* \bar{t}}, \tag{13a}$$

$$\bar{a}(\bar{x},\bar{t}) = \sum_{m=1}^{\infty} W_m(\bar{x}) \ddot{q}_m(\bar{t}) = \frac{4\pi^2}{(\kappa_1 L)^4} \sum_{m=1}^{\infty} \sum_{r=1}^{N_p} \frac{1}{1 - (\bar{\omega}_m/\bar{\omega}_r^*)^2} \int_0^1 W_m(\bar{x}) F_r(\bar{x})\, d\bar{x} W_m(\bar{x}) e^{i\bar{\omega}_r^* \bar{t}}. \tag{13b}$$

As in Eq. (6), two factors can be introduced as follows:

$$\mathrm{SF}_{\bar{w}}(m,r) = \frac{1}{\bar{\omega}_m^2 - \bar{\omega}_r^{*2}}, \quad \mathrm{SF}_{\bar{a}}(m,r) = \frac{1}{1 - (\bar{\omega}_m/\bar{\omega}_r^*)^2}. \tag{14}$$

To separate the spatial and temporal information from the beam response, it is useful to introduce several abbreviation notations as follows:

$$\bar{c}_{mr} = \int_0^1 W_m(\bar{x}) F_r(\bar{x})\, d\bar{x}, \tag{15}$$

$$\bar{g}_r^{\bar{w}}(\bar{x}) = \sum_{m=1}^{\infty} \bar{c}_{mr} \mathrm{SF}_{\bar{w}}(m,r) W_m(\bar{x}), \quad \bar{g}_r^{\bar{a}}(\bar{x}) = \sum_{m=1}^{\infty} \bar{c}_{mr} \mathrm{SF}_{\bar{a}}(m,r) W_m(\bar{x}). \tag{16}$$

With the help of the above notations, it is easy to recast Eq. (13) as

$$\bar{w}(\bar{x},\bar{t}) = \frac{4\pi^2}{(\kappa_1 L)^4} \sum_{r=1}^{N_p} \bar{g}_r^{\bar{w}}(\bar{x}) e^{i\bar{\omega}_r^* \bar{t}}, \quad \bar{a}(\bar{x},\bar{t}) = \frac{4\pi^2}{(\kappa_1 L)^4} \sum_{r=1}^{N_p} \bar{g}_r^{\bar{a}}(\bar{x}) e^{i\bar{\omega}_r^* \bar{t}}. \tag{17}$$

The reconstruction of the distributed dynamic loads from the beam response begins with the measured translational displacements denoted as

$$\bar{w}(\bar{x}_i,\bar{t}_n), \quad i = 1,\ldots,N_m, \quad n = 1,\ldots,N_T, \tag{18}$$

where N_m is the number of measurement locations along the beam and N_T the number of data in time dimension. From a simple frequency analysis, one reaches the dominate circular frequencies and the corresponding amplitudes contained in the response data denoted by

$$\bar{\omega}_r^*, \quad r = 1, \ldots, N_p, \quad \bar{g}_r^{\bar{w}}(x_i), \quad r = 1, \ldots, N_p, \quad i = 1, \ldots, N_m, \tag{19}$$

where N_p is the number of dominate frequencies, and $\bar{\omega}_r^*$ is sorted so that $\bar{\omega}_1^* < \cdots < \bar{\omega}_{N_p}^*$. The amplitude corresponding to the rth dominate circular frequency $\bar{\omega}_r^*$ yields

$$\bar{g}_r^{\bar{w}}(\bar{x}_i) = \sum_{m=1}^{\infty} \bar{c}_{mr} \mathrm{SF}_{\bar{w}}(m, r) W_m(\bar{x}_i), \quad i = 1, \ldots, N_m. \tag{20}$$

Now that the sets of $\bar{\omega}_r^*$ and $\bar{g}_r^{\bar{w}}(\bar{x}_i)$ are available, the scale factors $\mathrm{SF}_{\bar{w}}$ and $\mathrm{SF}_{\bar{a}}$ can be calculated, the limitation of the magnitude level of $\bar{c}_{mr}$ can be estimated, and the modes can be selected and denoted as a set B_m. If the number of modes in B_m is M, Eq. (20) can practically be given as a truncated form as follows:

$$\bar{g}_r^{\bar{w}}(\bar{x}_i) = \sum_{m \in B_m} \bar{c}_{mr} \mathrm{SF}_{\bar{w}}(m, r) W_m(\bar{x}_i), \quad i = 1, \ldots, N_m. \tag{21}$$

Eq. (21) may be an ill-posed problem for the solution of $\bar{c}_{mr}$. Consequently, the pseudo-inverse method or regularization approach, such as Tikhonov regularization [16,20,23], should be employed. When $\bar{c}_{mr}$ is solved from Eq. (21), the remaining problem is solving Eq. (15) for $F_r(\bar{x})$. Eq. (15) can be regarded as a mapping A from the space of all kinds of $F_r(\bar{x})$, denoted as U, to the space of all $W_m(\bar{x})$, denoted as V. That is, $A: U \to V$. Hence, Eq. (15) can be solved for $F_r(\bar{x})$ by using the projection method as below [24].

Let U_N be an N-dimensional subspace of U with a series of orthogonal base functions $\{\varphi_n(\bar{x})\}$ with respect to a given inner product, V_M be an M-dimensional subspace of V with a series of orthogonal base functions $\{W_m(\bar{x})\}$ having the inner product defined by $\langle W_i, W_j \rangle = \int_0^1 W_i(\bar{x}) W_j(\bar{x}) \, \mathrm{d}\bar{x}$, and the following relations hold:

$$U_N \subset U_{N+1} \subset \cdots \subset U, \quad V_M \subset V_{M+1} \subset \cdots \subset V. \tag{22}$$

The definition of a projection operator $Q_M: V \to V_M$ enables one to establish an approximate projection

$$Q_M A|_{U_N} : U_N \to V_M. \tag{23}$$

Therefore, Eq. (15) as an approximate projection (23) can easily be recast as the following matrix equation:

$$\bar{\mathbf{A}}\,\mathbf{a} = \bar{\mathbf{c}}, \tag{24}$$

where $\bar{\mathbf{A}} \equiv [\int_0^1 W_m(\bar{x}) \varphi_n(\bar{x}) \, \mathrm{d}\bar{x}]_{M \times N}$, $\bar{\mathbf{c}} \equiv \{\bar{c}_{mr}\}_{M \times 1}$, and $\mathbf{a} \equiv \{a_n\}_{N \times 1}$ are the coefficients in expression $F_r(\bar{x}) = \sum_{\varphi_n \in U_n} a_n \varphi_n(\bar{x})$. Solving Eq. (24) for $\mathbf{a}$ gives $F_r(\bar{x})$ through the following truncated expansion:

$$F_r(\bar{x}) = \sum_{\varphi_n \in U_n} a_n \varphi_n(\bar{x}). \tag{25}$$

3.2. Consistent spatial expression for distributed dynamic loads

In previous studies [11,14], as mentioned in the introduction, the modified modal functions were employed as base functions in order to describe the distributed dynamic loads on a structure as a truncated linear combination of base functions. Such a description, however, may conflict with the actual dynamic loads near the fixed boundaries of the structure. For example, either the modal functions or the modified modal functions of a beam always tend to be zero near any fixed boundary even though the dynamic loads on the beam may not vanish. Hence, it is impossible to use any linear combination of those base functions to describe the non-zero dynamic loads near the fixed boundary of a structure.

This study, therefore, explores the consistent spatial expression for distributed dynamic loads to cope with the problem. In fact, there are a great variety of base functions, such as orthogonal polynomials, for this purpose. The practice of authors indicates that the Legendre polynomials can offer a consistent spatial expression to describe the distributed dynamic loads.

3.3. Error evolution

The analysis of error evolution of the theory will follow the development of the reconstruction theory addressed in Section 3.1.

Let $\Delta\bar{w}(\bar{x}_i,\bar{t}_n)$ be the error in the experimental data $\bar{w}(\bar{x}_i,\bar{t}_n)$, $\Delta\bar{\omega}_r^*$ and $\Delta\bar{g}_r^{\bar{w}}(\bar{x}_i)$ be the errors corresponding to $\bar{\omega}_r^*$ and $\bar{g}_r^{\bar{w}}(\bar{x}_i)$ obtained from $\bar{w}(\bar{x}_i,\bar{t}_n)$ by using frequency analysis. As Eq. (21) is a truncated form, let $\Delta\tilde{g}_r^{\bar{w}}(\bar{x}_i)$ be the theoretical errors in $\bar{g}_r^{\bar{w}}(\bar{x}_i)$, and $\Delta\bar{g}_r^{\bar{w}}(\bar{x}_i)+\Delta\tilde{g}_r^{\bar{w}}(\bar{x}_i)$ be the resultant errors in $\bar{g}_r^{\bar{w}}(\bar{x}_i)$. Therefore, Eq. (21) is practically recast as

$$\bar{g}_r^{\bar{w}}(\bar{x}_i)+\Delta\bar{g}_r^{\bar{w}}(\bar{x}_i)+\Delta\tilde{g}_r^{\bar{w}}(\bar{x}_i)=\sum_{m\in B_m}\bar{c}_{m\ r}^{*}SF_{\bar{w}}^{*}(m,r)W_m^{*}(\bar{x}_i),\quad i=1,\ldots,N_m, \tag{26}$$

where $\mathrm{SF}_{\bar{w}}^{*}(m,r)$ includes the error $\Delta\mathrm{SF}_{\bar{w}}(m,r)$ resulting from the errors of $\bar{\omega}_r^*$ and $\bar{\omega}_m$, $W_m^*(\bar{x}_i)$ carries with the error of $\Delta W_m(\bar{x}_i)$ resulting from the error of $W_m(\bar{x})$. Eq. (26) can be recast in a matrix form as

$$\tilde{\mathbf{T}}\,\tilde{\mathbf{c}}=\tilde{\mathbf{g}}, \tag{27}$$

where

$$\begin{aligned}&\tilde{\mathbf{T}}\equiv[\mathrm{SF}_{\bar{w}}^{*}(m,r)W_m^{*}(\bar{x}_i)]_{N_m\times M},\ \tilde{\mathbf{c}}\equiv\{\bar{c}_{mr}^{*}\}_{M\times 1},\\ &\tilde{\mathbf{g}}\equiv\{\bar{g}_r^{\bar{w}}(\bar{x}_i)+\Delta\bar{g}_r^{\bar{w}}(\bar{x}_i)+\Delta\tilde{g}_r^{\bar{w}}(\bar{x}_i)\}_{N_m\times 1},\quad i=1,\ldots,N_m,\ m\in B_m.\end{aligned} \tag{28}$$

The Tikhonov regularization approach gives the regularized solution to Eq. (27)

$$\tilde{\mathbf{c}}_\alpha=(\tilde{\mathbf{T}}^{*}\times\tilde{\mathbf{T}}+\alpha\times\mathbf{I})^{-1}\times\tilde{\mathbf{T}}^{*}\times\tilde{\mathbf{g}}, \tag{29}$$

where the asterisk denotes conjugate transpose and α is the regularization parameter.

Suppose that the errors of $\tilde{\mathbf{T}}$ and $\tilde{\mathbf{g}}$ are bounded as

$$||\tilde{\mathbf{T}}-\mathbf{T}||\leqslant h,\quad ||\tilde{\mathbf{g}}-\mathbf{g}||\leqslant\delta, \tag{30}$$

where $||\bullet||$ represents a consistent norm. Then, the estimation of the error of $\tilde{\mathbf{c}}_\alpha$ is given by

$$||\tilde{\mathbf{c}}_\alpha-\mathbf{c}||\leqslant\frac{||\mathbf{T}^{+}||\times||\tilde{\mathbf{g}}||}{\sigma_{\min}}\times\alpha+||\mathbf{T}^{+}||\times\delta+\frac{\sqrt{5}}{2}\times\frac{h}{\alpha}\times(\delta^2+\alpha\times||\mathbf{c}||^2)^{1/2}, \tag{31}$$

where $\sigma_{\min}$ is the minimal eigenvalue of $\mathbf{T}^{*}\mathbf{T}$, $\tilde{\mathbf{c}}_\alpha$ the regularized solution, and $\mathbf{c}$ the theoretical solution [23]. The matrix $\mathbf{T}$ in (31) can be replaced by $\tilde{\mathbf{T}}$, with little loss of accuracy in practice.

Finally, according to the error theorem of the projection method [24], the error estimation of the solution of Eq. (24) for $\tilde{\mathbf{a}}$ is given by

$$||\tilde{\mathbf{a}}-\mathbf{a}||\leqslant||\tilde{\mathbf{c}}_\alpha-\mathbf{c}||\times||R_N||+||R_NA\mathbf{a}-\mathbf{a}||, \tag{32}$$

where $R_N\equiv(Q_MA|_{U_N})^{-1}Q_M: V\to U_N\subset U$, and $Q_MA|_{U_N}\equiv\tilde{\mathbf{A}}_{M\times N}$.

4. Case studies

This section presents two case studies first to demonstrate how the "mode selection" well supports the hypothesis of the optimal range for reconstructing distributed dynamic loads, and then gives another two case studies to show the accuracy of the improved theory on reconstructing the distributed dynamic loads and the effect near the fixed boundary.

All case studies in this section deal with a simply supported undamped Euler beam with length $L=1\,\mathrm{m}$, area of cross section $A=1.2\times10^{-3}\,\mathrm{m}^2$, second moment of area of cross section $I=3.6\times10^{-9}\,\mathrm{m}^4$, Young's modulus $E=2\times10^{11}\,\mathrm{N\,m}^{-2}$, and density $\rho=7800\,\mathrm{kg\,m}^{-3}$. Other parameters in the case studies are the time interval $T=10\,\mathrm{s}$, the sampling rate $\Delta t=0.1\,\mathrm{ms}$, the number of measures, and the position of measurements $N_x=16$, $x_i=iL/17$, $i=1,\ldots,16$. Some dimensionless parameters are the time length $\bar{T}\approx137.7680$, the sampling rate $\Delta\bar{t}\approx1.4\times10^{-3}$, and the position of measurements $\bar{x}_i=i/17$, $i=1,\ldots,16$.

In the case studies, the dimensionless translational displacements of the beam were sampled from the corresponding analytical solution, and only the steady-state responses were put into use since the components

of free vibration could easily be picked out for an undamped beam. To simulate measured data, the uniformly distributed random noises were added to the natural frequencies, mode shapes, and displacements, where an additive noise level within the upper bound of $\bar{\omega}_1/1000$ was applied to the dimensionless natural frequencies, a multiplicative noise level within the upper bound of $1/50$ to the dimensionless mode shapes, and a multiplicative noise level within the upper bound of 1×10^{-3} to the dimensionless translational displacements. However, no noise was applied to the dimensionless mode shapes when they were used as orthogonal base functions to reconstruct the distributed dynamic loads.

In mode selection, a threshold $\varepsilon_{\mathrm{SF}}$ was introduced. The modes satisfying the inequality $|\mathrm{SF}_{\bar{w}}(m,r)|/\max_{n\in D}(|\mathrm{SF}_{\bar{w}}(n,r)|)\geqslant\varepsilon_{\mathrm{SF}}(r)$ were selected and denoted as a set D_m for each dominate excitation frequency, where D is a set including enough modes under consideration. Moreover, in all case studies, the relative errors were defined as the absolute errors divided by the corresponding maximum.

The first and the second case studies are to demonstrate the effect of the "mode selection". In the first case study, the Euler beam was assumed to be subject to a harmonic excitation $\bar{f}(\bar{x},\bar{t})=\sum_{i=1,5,6,7,10}\bar{f}_i W_i(\bar{x})\sin(\bar{\omega}^*\bar{t})$, where $\bar{\omega}^*=\bar{\omega}_3+0.8\,\bar{\omega}_1$, $\bar{f}_i=1,\ \ i=1,5,6,7,10$. Fig. 2 shows how the scale factors $\mathrm{SF}_{\bar{w}}$ of the particular frequency varied with the order of the modes. The threshold $\varepsilon_{\mathrm{SF}}$ was empirically tried twice. At first, when $\varepsilon_{\mathrm{SF}}$ was set to 1×10^{-3}, the set $D_m=1\ldots11$ was selected. Fig. 3 shows the corresponding reconstruction results and errors, and indicates that the set D_m of selected modes covered all

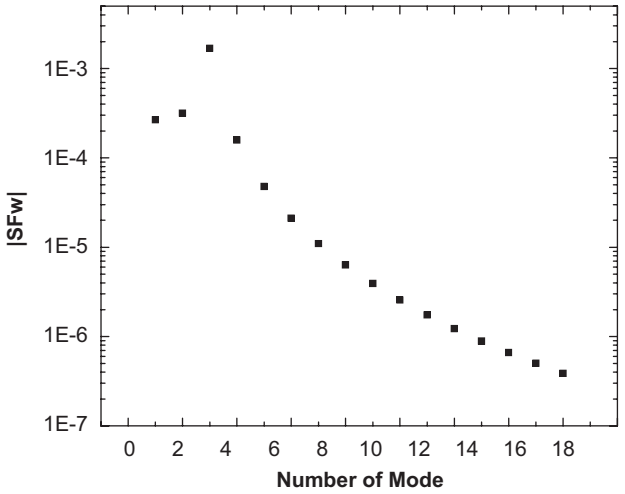

Fig. 2. $\mathrm{SF}_{\bar{w}}$ for case 1.

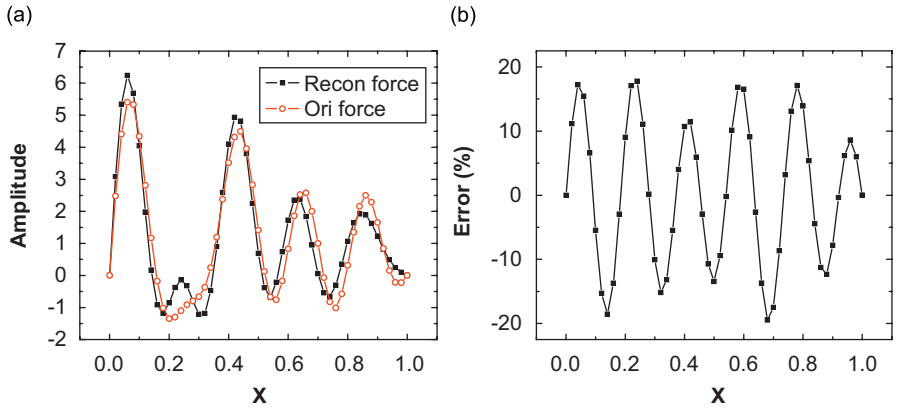

Fig. 3. Comparison between reconstructed and original loads for case 1, where $\varepsilon_{\mathrm{SF}}=1\times10^{-3}$, $D_m=1\ldots11$.

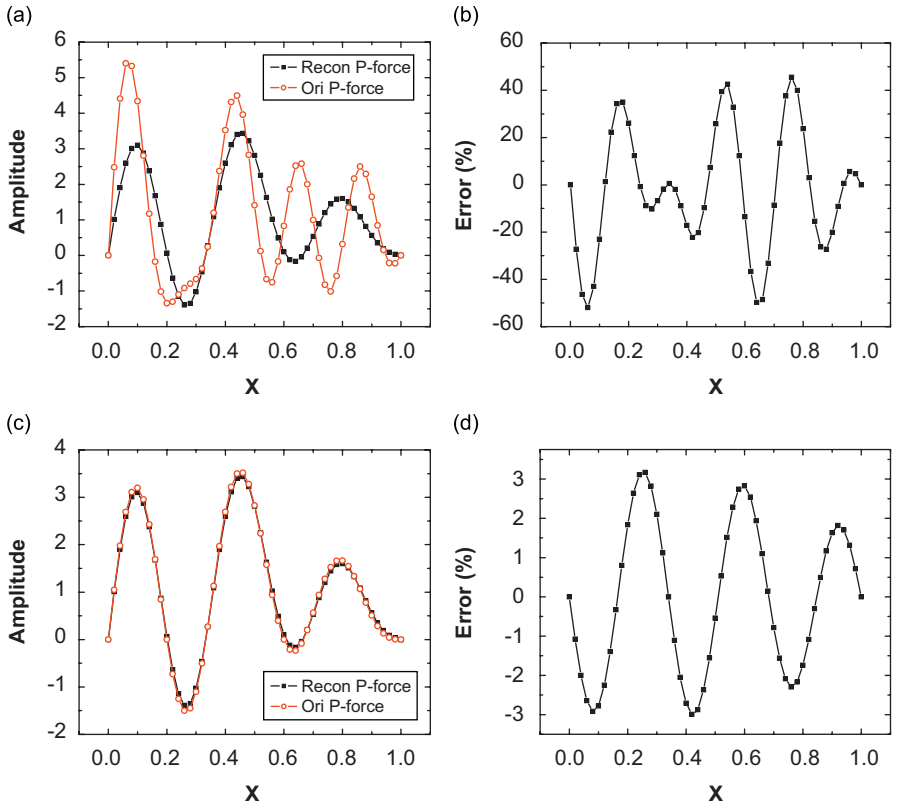

Fig. 4. Comparison between reconstructed and original loads for case 1, where $\varepsilon_{SF} = 1 \times 10^{-2}$, $D_m = 1 \ldots 6$.

spatial modes in the original load. Then, ε_{SF} was set to 1×10^{-2}, and the set $D_m = 1 \ldots 6$ was selected. In this case, D_m did not cover Modes 7 and 10 in the original load. Fig. 4 shows the reconstruction results and errors. Subfigures 4(a) and 4(b) give the comparison between the reconstructed load and the original load, whereas subfigures 4(c) and 4(d) are the comparison between the reconstructed load and the corresponding modal parts, namely, Modes 1, 5, and 6, in the original load. It is clear from Fig. 3(b) and 4(d) that the corresponding modal parts in the original load are accurately reconstructed when ε_{SF} is larger or the range of D_m is narrower. It is worthy to mention that the shapes of error curves are not important because they are influenced by the random errors.

The second case is to reconstruct the distributed dynamic loads with two harmonic components in the form $\bar{f}(\bar{x}, \bar{t}) = \sum_{i=1,5,9} \bar{f}_i W_i(\bar{x}) \sin(\bar{\omega}_1^* \bar{t}) + \sum_{j=2,6,13} \bar{f}_j W_j(\bar{x}) \sin(\bar{\omega}_2^* \bar{t})$, where $\bar{\omega}_1^* = \bar{\omega}_3 + 0.8\,\bar{\omega}_1$, $\bar{\omega}_2^* = \bar{\omega}_8 + 0.8\,\bar{\omega}_1$, and $\bar{f}_i = \bar{f}_j = 1$, $i = 1, 5, 9$, $j = 2, 6, 13$. Fig. 5 presents the variation of the scale factors $SF_{\bar{w}}$ of the two frequencies with regard to the order of the modes. Similarly, the threshold ε_{SF} was first set to 1×10^{-3}, $D_m(\bar{\omega}_1^*) = 1 \ldots 11$ and $D_m(\bar{\omega}_2^*) = 1 \ldots 16$ were selected, respectively. In this case, both sets $D_m(\bar{\omega}_1^*)$ and $D_m(\bar{\omega}_2^*)$ covered all spatial modes in the dynamic loads. Fig. 6 shows the reconstruction of the two components in (a) and (c), as well as the corresponding errors in (b) and (d). When the threshold ε_{SF} was set to 1×10^{-2}, then $D_m(\bar{\omega}_1^*) = 1 \ldots 6$ and $D_m(\bar{\omega}_2^*) = 1 \ldots 10$ were selected. The corresponding results did not cover some spatial modes in the distributed dynamic loads. Fig. 7 shows the reconstruction results and errors. Subfigures 7(a) and (b) give the comparison between the reconstructed and original loads of the first harmonic component, whereas subfigures 7(c) and (d) give the comparison between the reconstructed load and the corresponding modal parts in the original load of the first harmonic component. Subfigures 7(e) and (f) are the comparison between the reconstructed and original loads of the second harmonic component, whereas subfigures 7(g) and (h) are the comparison between the reconstructed load and the corresponding modal parts of the original load of the second harmonic component. The comparison of subfigures 7(d) and (h) to subfigures 6(b) and (d)

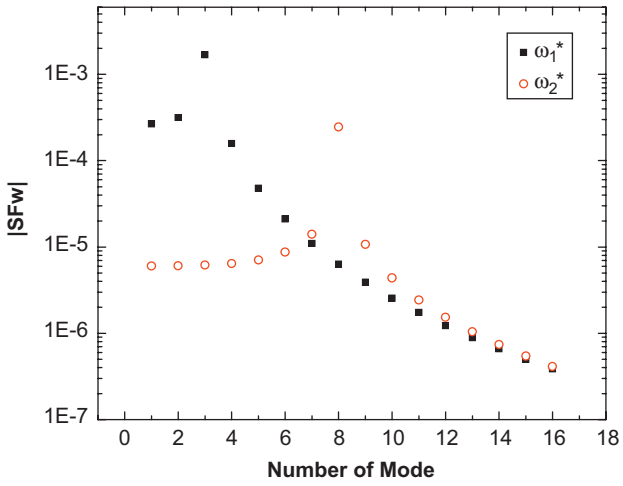

Fig. 5. $SF_{\bar{w}}$ for case 2.

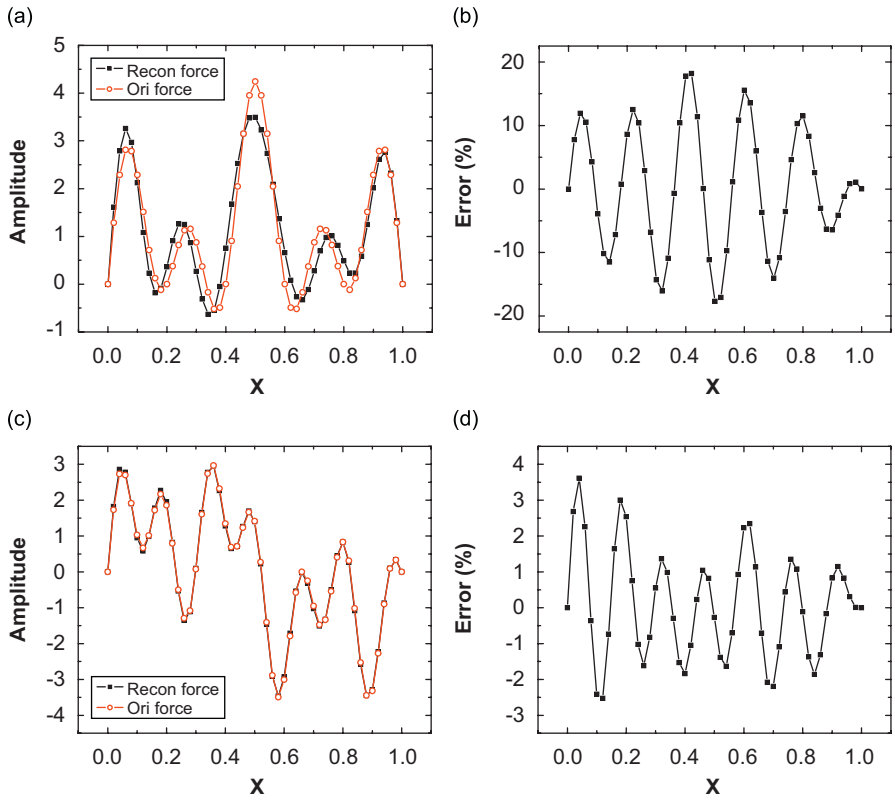

Fig. 6. Comparison between reconstructed and original loads for case 2, where $\varepsilon_{SF} = 1 \times 10^{-3}$, $D_m(\bar{\omega}_1^*) = 1 \ldots 11$, $D_m(\bar{\omega}_2^*) = 1 \ldots 16$.

indicates that a narrower range of selected modes enhances the reconstruction accuracy. However, it is not true that the narrower the range of selected modes, the higher the accuracy of the reconstruction. Therefore, an optimal range for "mode selection" is really expected.

In the above two cases $\{\varphi_n(\bar{x})\}$ were taken as the normalized natural mode functions $\{W_m(\bar{x})\}$, whereas in the following two cases $\{\varphi_n(\bar{x})\}$ were taken as the normalized modified Legendre polynomials on interval (0, 1)

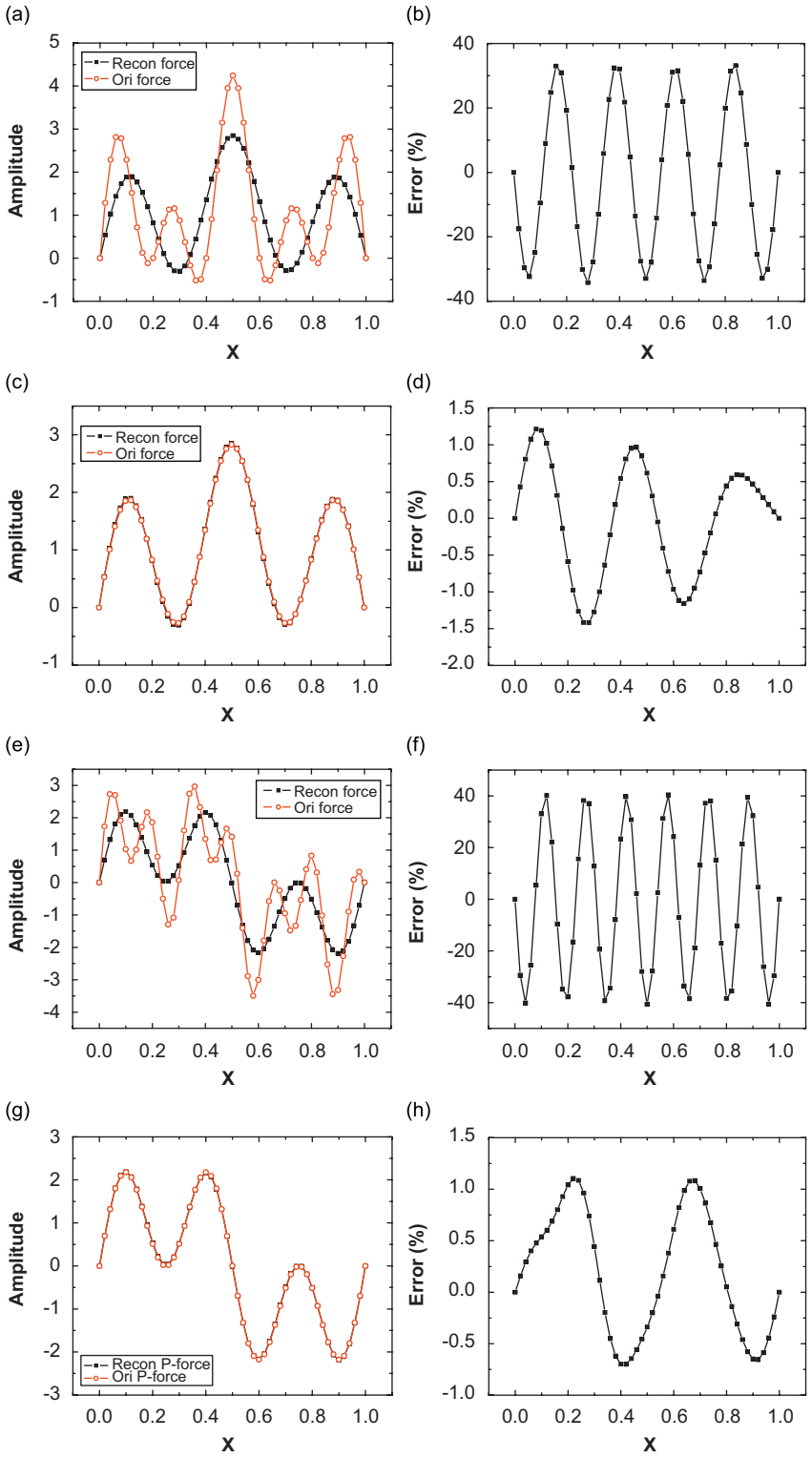

Fig. 7. Comparison between reconstructed and original loads for case 2, where $\varepsilon_{SF} = 1 \times 10^{-2}$, $D_m(\bar{\omega}_1^*) = 1 \ldots 6$, $D_m(\bar{\omega}_2^*) = 1 \ldots 10$.

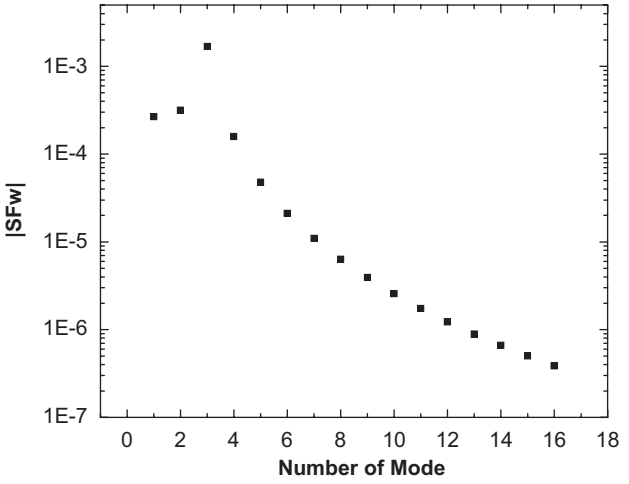

Fig. 8. $SF_{\bar{w}}$ for case 3.

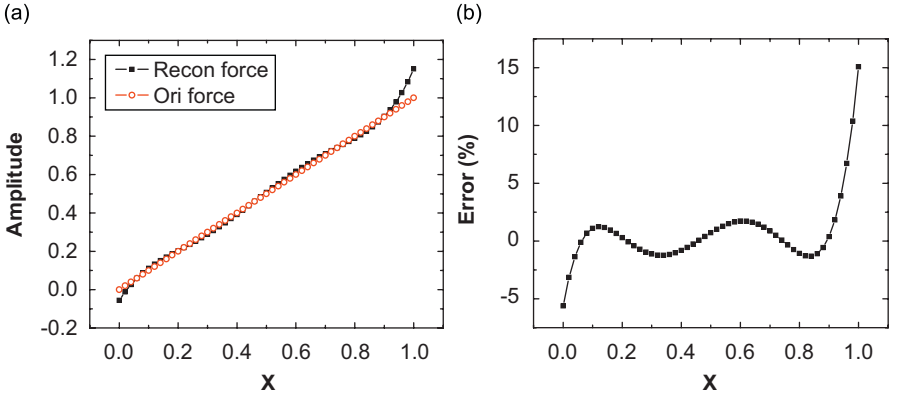

Fig. 9. Comparison between reconstructed and original loads for case 3, where $\varepsilon_{SF} = 1 \times 10^{-2}$, $D_m = 1 \ldots 6$.

so as to reconstruct the distributed dynamic loads, which may not vanish near the fixed boundary of the beam. For the purpose of comparison, the number of polynomials $\{\varphi_n(\bar{x})\}$ remained the same as the number of modes $\{W_m(\bar{x})\}$ in the following two case studies.

In the third case study, the load to be reconstructed is a distributed harmonic excitation in the form $\bar{f}(\bar{x}, \bar{t}) = \bar{f}_0 \bar{x} \sin(\bar{\omega}^* \bar{t})$, where $\bar{\omega}^* = \bar{\omega}_3 + 0.8\,\bar{\omega}_1$, $\bar{f}_0 = 1$. Fig. 8 shows the scale factors $SF_{\bar{w}}$. In this case, the threshold was set to $\varepsilon_{SF} = 1 \times 10^{-2}$, and the set $D_m = 1 \ldots 6$ was selected. Fig. 9 shows the comparison between the reconstructed and original loads, as well as the errors. The figure indicates the high accuracy of the distributed dynamic loads in the middle part of the beam and the acceptable errors of the distributed dynamic loads near the fixed boundaries.

The final case study is to reconstruct the distributed dynamic loads in the form $\bar{f}(\bar{x}, \bar{t}) = \bar{f}_1 \bar{x} \sin(\bar{\omega}_1^* \bar{t}) + \bar{f}_2 \bar{x}^3 \sin(\bar{\omega}_2^* \bar{t})$, where $\bar{\omega}_1^* = \bar{\omega}_1 + 0.8\,\bar{\omega}_1$, $\bar{\omega}_2^* = \bar{\omega}_3 + 0.8\,\bar{\omega}_1$, $\bar{f}_1 = \bar{f}_2 = 1$. Fig. 10 shows the scale factors $SF_{\bar{w}}$ in this case. The threshold for "mode selection" was set to $\varepsilon_{SF} = 1 \times 10^{-2}$, and the sets $D_m(\bar{\omega}_1^*) = 1 \ldots 3$, $D_m(\bar{\omega}_2^*) = 1 \ldots 6$ were determined. Fig. 11 shows the comparison between the reconstructed and original loads, as well as the errors. Similarly, the reconstructed loads are relatively accurate in the middle part of the beam, while the reconstruction errors near the fixed boundaries increase but are acceptable.

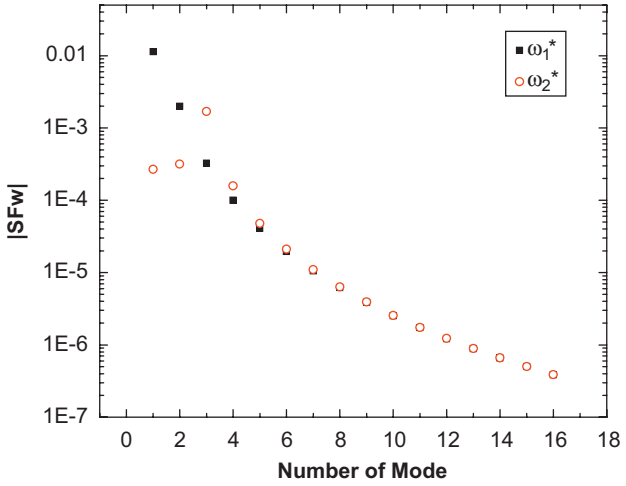

Fig. 10. $SF_{\bar{w}}$ for case 4.

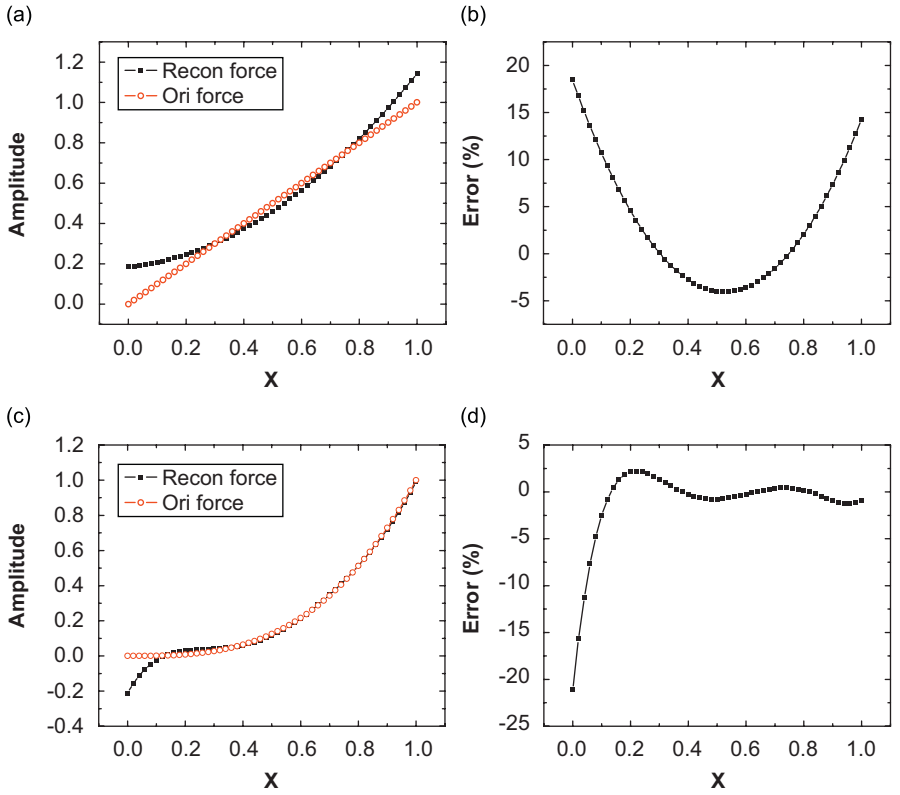

Fig. 11. Comparison between reconstructed and original loads for case 4, where $\varepsilon_{SF} = 1 \times 10^{-2}$, $D_m(\bar{\omega}_1^*) = 1 \ldots 3$, $D_m(\bar{\omega}_2^*) = 1 \ldots 6$.

In the third and fourth cases, the reconstruction errors become profound near the fixed boundaries. However, the errors near the fixed boundaries can be greatly decreased due to the application of the "consistent spatial expression" based on the series of Legendre polynomials. Nevertheless, the relatively large reconstruction errors near the fixed boundary remain an open and tough problem.

5. Concluding remarks

In this study, two scale factors, $SF_{\bar{w}}$ and $SF_{\bar{a}}$, are put forward first from a viewpoint of forward dynamics for reconstructing the distributed dynamic loads on an Euler beam. Similar scale factors can naturally be introduced in reconstructing the distributed dynamic loads on other kinds of structures. Based on the scale factors, an idea of "mode selection" is proposed so as to reach the optimal range of frequency and spatial modes for reconstructing the distributed dynamic loads.

In the previous studies of reconstructing the dynamic loads on a beam [11,14], the modified modal functions were employed to describe the distributed dynamic loads in a linear combination of those functions. However, the modal functions, including the modified modal functions, tend to vanish near the fixed boundary where the dynamic loads may not be zero. Therefore, it is better to use "the consistent spatial expression" for the distributed dynamic loads to be reconstructed.

Based on the ideas of "mode selection" and "consistent spatial expression for distributed dynamic loads", an improved theory is addressed to reconstruct the distributed dynamic loads on an Euler beam. The numerical simulations show that the accuracy of reconstructed loads, even near the fixed boundaries, can be greatly increased by using "mode selection" and "consistent spatial expression for distributed dynamic loads".

There are still some open problems for further investigation. For instance, it is worthwhile to give the threshold ε_{SF} analytically. Though the reconstruction accuracy near the fixed boundaries is greatly enhanced, it is much worse than the accuracy in the middle interval.

References

[1] L.A. Lifschitz, C.E. D'Attellis, Input force reconstruction using wavelets with applications to a pulsed plasma thruster, *Mathematical and Computer Modelling* 41 (4–5) (2005) 361–369.

[2] J. Liu, C. Ma, I. Kung, D. Lin, Input force estimation of a cantilever plate by using a system identification technique, *Computer Methods in Applied Mechanics and Engineering* 190 (11–12) (2000) 1309–1322.

[3] M.T. Martin, J.F. Doyle, Impact force identification from wave propagation responses, *International Journal of Impact Engineering* 18 (1) (1996) 65–77.

[4] D.C. Kammer, Input force reconstruction using a time domain technique, AIAA-96-1201-CP.

[5] T.H.T. Chan, D.B. Ashebo, Theoretical study of moving force identification on continuous bridges, *Journal of Sound and Vibration* 295 (3–5) (2006) 870–883.

[6] S.S. Law, Y.L. Fang, Moving force identification: optimal state estimation approach, *Journal of Sound and Vibration* 239 (2) (2001) 233–254.

[7] E.G. Yanyutin, A.V. Voropai, Identification of the impulsive load on an elastic rectangular plate, *International Applied Mechanics* 39 (10) (2003) 1199–1204.

[8] M. De Araújo, J. Antunes, P. Piteau, Remote identification of impact forces on loosely supported tubes—part 1: basic theory and experiments, *Journal of Sound and Vibration* 215 (5) (1998) 1015–1041.

[9] N.S. Vyas, A.L. Wicks, Reconstruction of turbine blade forces from response data, *Mechanism and Machine Theory* 36 (2) (2001) 177–188.

[10] M.C. Djamaa, N. Ouelaa, C. Pezerat, J.L. Guyader, Reconstruction of a distributed force applied on a thin cylindrical shell by an inverse method and spatial filtering, *Journal of Sound and Vibration* 301 (3–5) (2007) 560–575.

[11] Yi. Liu, W.S. Shepard Jr., An improved method for the reconstruction of a distributed force acting on a vibrating structure, *Journal of Sound and Vibration* 291 (1–2) (2006) 369–387.

[12] N. Sehlstedt, A well-conditioned technique for solving the inverse problem of boundary traction estimation for a constrained vibrating structure, *Computational Mechanics* 30 (3) (2003) 247–258.

[13] C. Pezerat, J.L. Guyader, Force analysis technique: reconstruction of force distribution on plates, *Acta Acustica* 86 (2000) 322–332.

[14] S. Granger, L. Perotin, An inverse method for the identification of a distributed random excitation acting on a vibrating structure—part 1: theory, *Mechanical Systems and Signal Processing* 13 (1) (1999) 53–65.

[15] H.G. Choi, A.N. Thite, David J. Thompson, Comparison of methods for parameter selection in Tikhonov regularization with application to inverse force determination, *Journal of Sound and Vibration* 304 (2007) 894–917.

[16] H.G. Choi, A.N. Thite, D.J. Thompson, A threshold for the use of Tikhonov regularization in inverse force determination, *Applied Acoustics* 67 (7) (2006) 700–719.

[17] F.E. Gunawan, H. Homma, Y. Kanto, Two-step B-splines regularization method for solving an ill-posed problem of impact-force reconstruction, *Journal of Sound and Vibration* 297 (1–2) (2006) 200–214.

[18] J.W. Hilgers, B.S. Bertram, Comparing different types of approximators for choosing the parameters in the regularization of ill-posed problems, *Computers and Mathematics with Applications* 48 (2004) 1779–1790.

[19] D. Calvetti, S. Morigi, L. Reichel, F. Sgallari, Tikhonov regularization and the L-curve for large discrete ill-posed problems, *Journal of Computational and Applied Mathematics* 123 (2000) 423–446.
[20] S.H. Yoon, P.A. Nelson, Estimation of acoustic source strength by inverse methods: part II, experimental investigation of methods for choosing regularization parameters, *Journal of Sound and Vibration* 233 (4) (2000) 669–705.
[21] H. Lee, Y. park, Error analysis of indirect force determination and a regularization method to reduce force determination error, *Mechanical Systems and Signal Processing* 9 (6) (1995) 615–633.
[22] K. Mosegaard, A. Tarantola, Monte Carlo sampling of solutions to inverse problems, *Journal of Geophysical Research* 100 (B7) (1995) 12,431–12,447.
[23] F. Kunert, *Pseudoinverse Matrizen und die Methode der Regularisierung*, Teubner-Texte zur Mathematik, Leipzig, 1976.
[24] T.Y. Xiao, S.G. Yu, Y.F. Wang, *Numerical Approaches to Inverse Problems*, Science Press, Beijing, 2003 (in Chinese).